

# Quantitative Evaluation of LiFePO<sub>4</sub> Battery Cycle Life Improvement Using Ultracapacitors

Chen Zhao, *Student Member, IEEE*, He Yin, *Student Member, IEEE*, Chengbin Ma, *Member, IEEE*

**Abstract**—This letter develops a systematic approach to quantitatively evaluate and compare LiFePO<sub>4</sub> battery cycle life improvement using ultracapacitors (UCs). The impact of UC sizing on temperature rise, capacity loss, and power fade under a real dynamic load profile are included for a comprehensive discussion and evaluation. It is found that the cycle-related battery capacity losses are reduced by 28.6% (C/3) and 29.0% (1C) using the optimized number of UCs, while the reductions are 36.3% (C/3) and 39.3% (1C) assuming an infinite number of UCs. The reductions on the power fade are 23.6% and 57.3% for the cases with optimized and infinite numbers of UCs, respectively. The reductions on temperature rise, 1.38 °C and 1.93 °C, in the two cases are also observed when discharging from 80% to 30% SOC in one test cycle. The developed approach in the letter could serve as a general procedure to evaluate the cycle life improvement for other types of batteries when combined with UCs.

**Index Terms**—Battery, Ultracapacitor, Cycle life, Hybrid energy storage system, Testing

## I. INTRODUCTION

Lithium-ion batteries are now one of the most popular energy storage devices for electric vehicles (EVs). Meanwhile, frequent starts and stops in the city driving degrade the cycle life of the batteries. One possible solution is through the hybridization of batteries and ultracapacitors (UCs). In the battery-UC hybrid energy storage system (HESS) the high-power-density and high-efficiency UCs work as an energy buffer to smooth the battery power, and thus the battery cycle life could be prolonged [1], [2]. This aspect was investigated through simulation-based discussions using the static battery cycle life models [3], [4]. These models were developed based on the ageing test under constant operating conditions, i.e., static load profiles. However, they can not accurately reflect the cycle life of the batteries under a dynamic load profile. A semi-empirical dynamic battery cycle life model was recently proposed for the capacity loss evaluation under pulsed load profiles [5]. The model does not include the influence of the load current, and the pulsed profiles are with day-long slow dynamics. The effect of the UC-modified plug-in hybrid electric vehicle load profile on LiMn<sub>2</sub>O<sub>4</sub> battery performance degradation was studied through the cycle life test [6]. Meanwhile, LiFePO<sub>4</sub> batteries are well known for their excellent cycling and thermal stabilities, and low cost [7], [8]. Initial discussion on the capacity loss reduction of the LiFePO<sub>4</sub> batteries using UCs can be found in [9]. However, the

impact of UC sizing on battery power fade, and temperature rise need to be further investigated for a comprehensive and quantitative evaluation. The purpose of this letter is to develop a systematic approach that evaluates and compares LiFePO<sub>4</sub> battery cycle life improvement under a real dynamic load profile, and with different numbers of UCs.

## II. EXPERIMENTAL APPROACH

In this section the number of UCs is first optimized that minimizes the energy consumption under a dynamic load profile. Then accelerated cycle life test is designed to compare the battery degradation in three cases, i.e., without using UCs, with optimized number of UCs and ideal infinite number of UCs.

### A. Sizing of UC Pack

Here the capacitor semi-active hybrid is used, in which a dc-dc converter connects the UC pack and the load [10]. This topology enables the decoupling between the UC and battery voltages, and thus improves the utilization of UC energy. A first-order low-pass filter based control strategy is used to determine the load power distribution between the battery and UC packs [1]. Due to its well-known high power density, the UC pack provides the high-frequency components of the original dynamic load profile through the dc-dc converter, while the remaining low-frequency components after the filtering are supplied by the battery pack. An optimization problem is then formulated to solve the number (i.e., sizing) of UC cells in series,  $N_u$ , and the cut-off frequency of the first-order low-pass filter,  $f_c$ , that minimize the energy consumption,  $E_c$ , under a target dynamic load profile, JC08 driving cycle here (the Japanese urban test cycle representing congested city driving conditions) in Fig. 1.

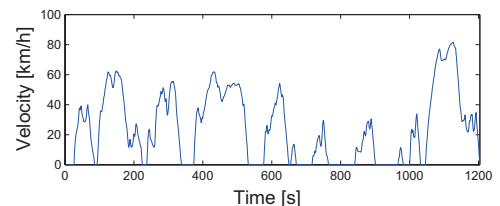


Fig. 1. Velocity profile of the JC08 driving cycle.

The total energy consumption,  $E_c$ , can be calculated as

$$\min_{N_u, f_c} E_c = \frac{M_v + M_b + M_d + M_u}{M_v} E_b + E_{loss}, \quad (1)$$

where  $M_b$ ,  $M_d$ ,  $M_u$  are masses of the battery pack, the dc-dc converter, and the UC pack, respectively, and  $E_b$  is the energy consumption at the base vehicle mass  $M_v$ , 1100 kg, in

Manuscript received September 20, 2015; revised October 12, 2015; accepted November 10, 2015. This work was supported by the National Science Foundation of China under Grant 51375299 (2014–2017) and in part by Nippon Chemi-con Corporation. C. Zhao, H. Yin, and C. Ma are with Univ. of Michigan-Shanghai Jiao Tong Univ. Joint Institute, Shanghai Jiao Tong University, Shanghai, P. R. China (e-mail: zc437041363@sjtu.edu.cn; yyy@sjtu.edu.cn; chbma@sjtu.edu.cn). C. Ma is also with the School of Mechanical Engineering, Shanghai Jiao Tong University, Shanghai 200240, China.

a single JC08 driving cycle. The energy loss from the battery-UC HESS,  $E_{loss}$ , is

$$E_{loss} = \sum_{n=1}^N i_{b,n}^2 R_b T_s + \sum_{n=1}^N i_{d,n}^2 (R_d + R_u) T_s, \quad (2)$$

where  $i_{b,n}$  and  $i_{d,n}$  are currents of the battery pack and the dc-dc converter at the  $n$ th sampling instant and  $T_s$  is the sampling interval, 1 s here. The resistances,  $R_b$ ,  $R_d$ , and  $R_u$ , are the equivalent series resistances of the battery pack, the dc-dc converter, and the UC pack, respectively. They can be calculated as [11]

$$R_b = \frac{V_{bus}^2 (1 - \eta_b)}{S_b M_b}, \quad R_d + R_u = \frac{V_{bus}^2 (1 - \eta_d \eta_u)}{S_u M_u}, \quad (3)$$

where  $S$  and  $\eta$  denote the power density and efficiency of each component, respectively. The dc bus voltage,  $V_{bus}$ , is 330 V here. Table I shows the parameters of the battery and UC cells. For the dc-dc converter, its power density and efficiency,  $\eta_d$ , are 5300 W/kg and 98%, respectively, which are from [12]. The battery cells used in the following cycle life test are high energy density prismatic-type LiFePO<sub>4</sub> batteries. Thus the internal resistance of the battery cells is relatively high [13].

As illustrated in Fig. 2, the optimal values of  $N_u$  and  $f_c$  under the JC08 driving cycle are 160 and 0.005 Hz, respectively. Fig. 3 shows the battery power in the three cases. With optimized number of UCs the peak power (green curve) from the battery pack is significantly reduced, while in the ideal case where the number of the UCs is infinite, the battery pack only needs to supply the average load power (red line) of the test cycle because the energy stored in the UC pack is sufficient to supply the entire dynamic load power.

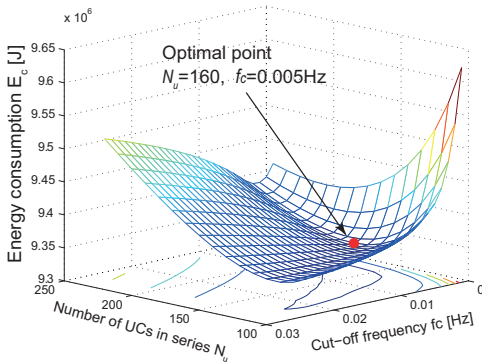


Fig. 2.  $E_c$  versus  $N_u$  and  $f_c$ .

TABLE I  
PARAMETERS OF BATTERY AND UC CELLS.

	Capacity	Voltage	Resistance	Mass	Power density <sup>1</sup>
Battery	12 Ah	3.2 V	8 m $\Omega$	0.37 kg	164 W/kg
UC	1200 F	2.5 V	0.8 m $\Omega$	0.28 kg	785 W/kg

### B. Cycle Life Test

Four 12-Ah Lishen LP2770102AC LiFePO<sub>4</sub> battery cells (No. 1–4) are used as test samples [see Table II]. Note in

<sup>1</sup>Power densities at 95% efficiency [14].

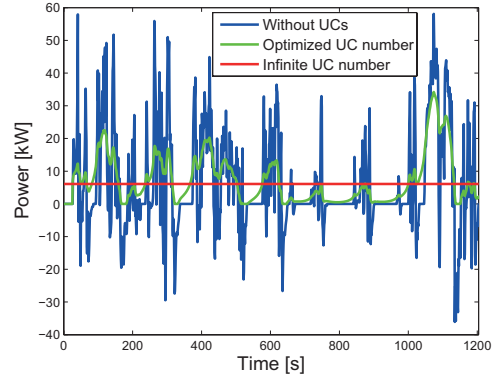


Fig. 3. Battery power in the three cases, without using UCs, optimized number of UCs, and infinite number of UCs.

TABLE II  
TEST METRICS.

Battery Cell	No. 1	No. 2	No. 3	No. 4
Number of UCs	None	Optimized	Infinite	None(Calendar life)

the test the No. 1–3 cells are cycled under the corresponding scaled down power profiles in Fig. 3. Real UCs and dc-dc converters are not used, as same as the test in [6]. The No. 4 cell is tested for the battery calendar life at 60% state of charge (SOC). In a single test cycle (scaled-down four continuous JC08 driving cycles) No.1–3 cells are discharged from 80% to 30% SOC, usually the usable SOC range of batteries in EV applications, and then rest for 20 minutes [15]. Next the three cells are charged back to 80% SOC at 1C current and rest for another 20 minutes. The four cells are all tested at 45 degrees centigrade in order to accelerate the battery ageing and thus shorten the test duration.

Before starting the cycle life test and after every 80 test cycles, the characteristics of the four cells are measured at 25 degrees centigrade using the reference performance test (RPT) [6]. The RPT consists of a pulse current test and two capacity tests at C/3 and 1C currents. In the pulse current test the fully charged battery is discharged at C/3 current with 10% capacity reduction and rests for 1 hour. This test sequence is repeated until the battery reaches the cut-off voltage, 2 V here.

### C. Experimental Setup

Figs. 4 shows the experimental setup and the schematic diagram of the accelerated cycle life test. The specifications of the experimental setup are listed in Tab. III. Three sets of power supply and electronic load are controlled by the LabVIEW program to charge and discharge the No. 1–3 cells. Five K-type thermocouples (i.e., temperature sensors) are attached to the surface of each cell (No. 1–3) [see Fig. 4] [16]. The measurement sensitivity and error of the NI 9213 DAQ module at room temperature are 0.02  $^{\circ}$ C and 1  $^{\circ}$ C, respectively, when using the K-type thermocouples. Fig. 5 shows the average values of the measured temperatures of No.1–3 cells when the cells are discharged from 80% to 30% SOC in a test cycle. The average temperature rises,  $\Delta T$ , in No. 2–3 cells are reduced by 1.38  $^{\circ}$ C and 1.93  $^{\circ}$ C, respectively, compared to that in

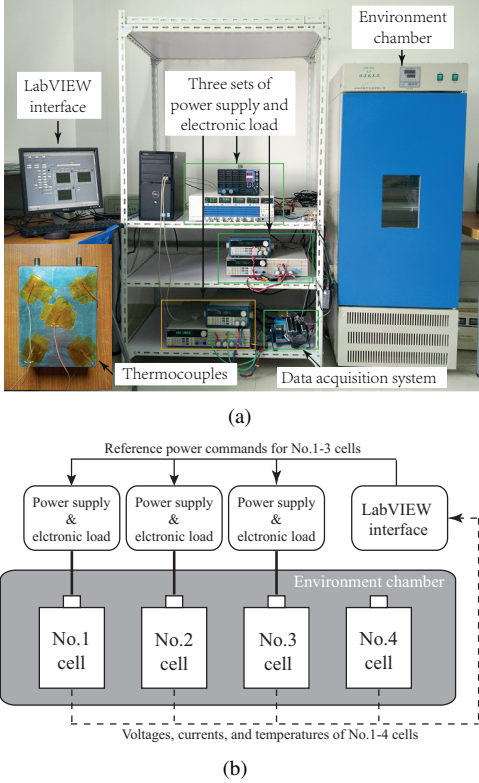


Fig. 4. Experimental setup. (a) Photo. (b) Schematic diagram.

the No. 1 cell. This advantage may potentially alleviate the difficulties in battery thermal management.

TABLE III  
SPECIFICATIONS OF EXPERIMENTAL SETUP.

Power supplies	
(Takasago ZX-800L-No. 1)	Max 800 W, 0–80 V, 0–80 A
(2 Maynuo M8852-No. 2, 3)	Max 600 W, 0–30 V, 0–20 A
Electronic loads	
(Kikusui PLZ-50F/150U-No. 1)	Max 600 W, 1.5–150 V, 0–120 A
(2 Maynuo M9711-No. 2, 3)	Max 150 W, 0–150 V, 0–30 A
Data acquisition system	
(NI 9213 (temperature))	NI 9213 (temperature)
(NI cDAQ-9174)	NI 9219 × 2 (voltage and current)
Environment chamber	
(Ruihua LRH-250)	Temperature range: -10–60 °C
	Accuracy: ±0.5 °C
Thermocouples (Fluke TT-K-30)	Insulation range: -267–260 °C

It is interesting to note that the temperatures of the No. 2 and 3 cells using UCs can be lower than the initial battery temperature of a test cycle, 45.5 °C in Fig. 5. This phenomenon is caused by a larger influence of the reversible entropic heat than that of the irreversible heat generated from the resistive dissipation at small currents and high temperatures [17][refer to Fig. 3]. Since the sign for reversible entropic heat is negative during discharge, the two cells using UCs undergo endothermic reactions, and thus their temperatures can be lower than 45.5 °C.

### III. RESULTS OF CYCLE LIFE TEST

#### A. Capacity Loss

In the cycle life test 1200 cycles were conducted using about one year, as shown in Fig. 6. Assuming that the capacity

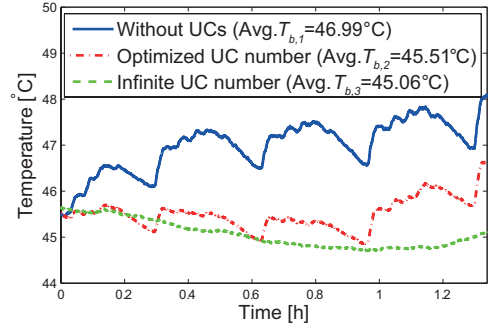


Fig. 5. The temperature variations in the No.1–3 cells (one test cycle).

loss brought by the cycling is independent of that due to the calendar time, the cycle-related capacity losses are calculated by removing the capacity loss of the No. 4 cell, as listed in Table IV [6]. Results show that with the optimized number of UCs, the cycle-related capacity losses at C/3 and 1C currents,  $Q_{C/3}^*$  and  $Q_{1C}^*$ , can be reduced by 28.6% and 29.0% respectively. In the ideal case with infinite number of UCs, the cycle-related capacity losses at C/3 and 1C currents are reduced by 36.3% and 39.3%, respectively. This trend matches the temperature rise in No. 1–3 cells, as shown in Fig. 5.

TABLE IV  
CYCLE-RELATED CAPACITY LOSSES OF FOUR CELLS AFTER 1200 CYCLES.

Number of UCs	None	Optimized	Infinite
$Q_{C/3}^*$	9.1%	6.5%	5.8%
$Q_{1C}^*$	10.7%	7.6%	6.5%

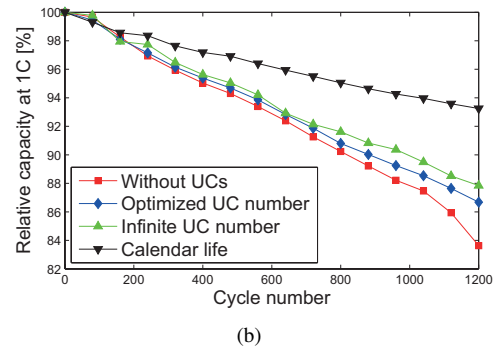
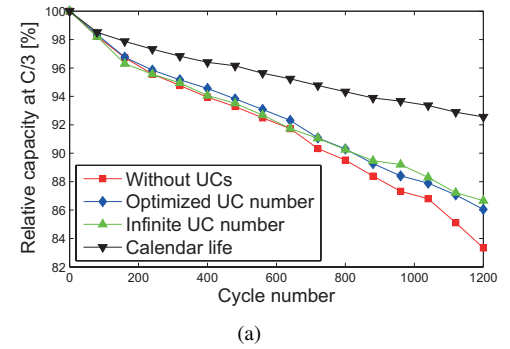


Fig. 6. Cell capacities versus cycle number. (a) C/3 current. (b) 1C current.

#### B. Power Fade

The data from a pulse current test is used to calculate the 10 s discharge resistance,  $R_{b,10s}$ , and pulse power capability

(PPC) [6], [18]. The two parameters are defined as follows,

$$R_{b,10s} = \frac{V_{t_0} - V_{t_1}}{I_{t_0} - I_{t_1}}, \quad PPC = \frac{(V_{t_0} - V_{min})V_{min}}{R_{b,10s}}, \quad (4)$$

where  $V$  and  $I$  are battery cell voltage and current, respectively. Here  $V_{min}$  is the minimum voltage of the battery cell. The measured voltage/current and time,  $t_0$  and  $t_1$ , are shown in Fig. 7. Note the open circuit voltage (OCV),  $V_{t_0}$ , only relates to the SOC and temperature of a battery. Besides, it is known that the trend of  $R_{b,10s}$  is similar despite different discharge currents [5], [19]. In the pulse current test high discharge currents may lead to unwanted battery degradation that adversely impacts the accuracy of the evaluation [20]. Thus the 10 s discharge resistance at C/3 current and the OCV at 50% SOC are used to evaluate the power fade.

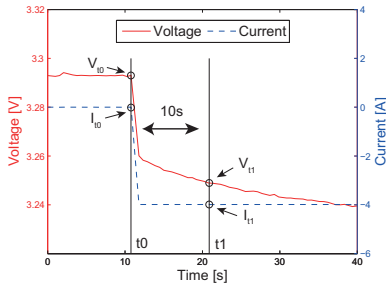
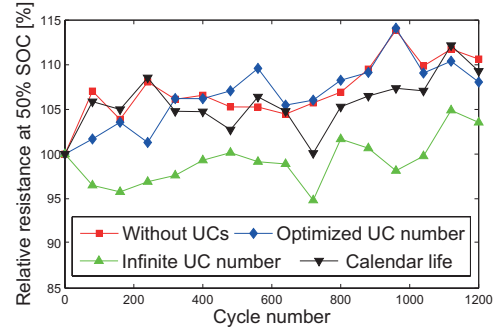


Fig. 7. Voltage and current of the battery cell in the pulse current test.

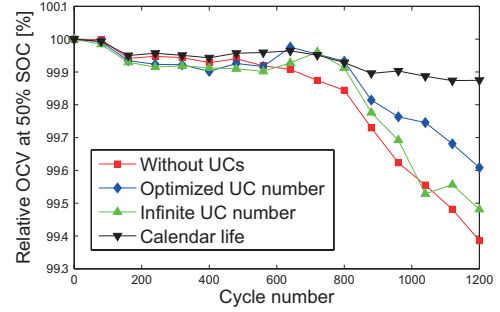
1) *Resistance Increase*: Fig. 8(a) shows that the variations of resistance of the battery cells are large, possibly due to the high-frequency dynamics of the voltage responses and the unavoidable measurement error in the mΩ range [19]. But the general trend shows that the resistance increases with the ageing of the cell. Because of the large variations of the resistances, in Fig. 8(a) the blue curve (optimized UC number) demonstrates nearly the same increase as the red curve (without UCs). However, Table V still shows that, after 1200 cycles, the resistance increase in the two cases using UCs is smaller than that in the other two cases.

2) *Open Circuit Voltage Drop*: As shown in Fig. 8(b), the OCV drops in No. 1–3 cells basically follow a similar trend. However, No. 2 and 3 cells still show improvements compared to No. 1 cell. In all the four cases the variations of OCV at 50% SOC are relatively small, especially during the first 600 cycles. Since the OCV drops after 1200 cycles are all small, the impact on OCV drop using UCs is limited, as summarized in Table V. Note the voltage reading accuracy of the NI 9219 DAQ module is  $\pm 0.3\%$ . The green curve (infinite UC number) in Fig. 8 actually shows a larger OCV drop than that of the blue curve (optimized UC number). This counter intuitive result is mostly caused by the measurement error. For example, the OCV drops in No. 1–4 cells after 1200 cycles are 0.0203 V, 0.0129 V, 0.0171 V, and 0.0041 V, respectively, with a measurement error of about  $0.0096 (= 3.2 \times 0.3\%)$  V.

3) *Pulse Power Capability Fade*: Because the OCV drops are relatively small, PPC fade is mainly determined by the resistance increase. As shown in Table V, the reductions on PPC fade are 23.6% and 57.3% in No. 2 and 3 cells, respectively. Using UCs, the PPC fade of the battery cell under cycling is even smaller than that in the calendar life test.



(a)



(b)

Fig. 8. 10 s discharge resistance  $R_{b,10s}$  and OCV of the four cells versus the cycle number. (a) 10 s discharge resistance  $R_{b,10s}$ . (b) OCV.

TABLE V  
PPC FADE OF FOUR BATTERY CELLS AFTER 1200 CYCLES.

Number of UCs	None	Optimized	Infinite	None (Calendar)
$\Delta R_{d,10s}$ (50% SOC)	10.6%	8.1%	3.5%	9.3%
$\Delta OCV$ (50% SOC)	0.6%	0.4%	0.5%	0.1%
$\Delta PPC$ (50% SOC)	11.0%	8.4%	4.7%	8.8%

## IV. CONCLUSION

This paper develops a systematic approach to experimentally evaluate the LiFePO<sub>4</sub> battery cycle life improvement using UCs. Particularly, the impact of the UC sizing on temperature rise, capacity loss, and power fade are quantitatively investigated. The improvements using UCs are observed that demonstrate the promising aspect of UCs to prolong the battery cycle life. It is interesting to note that in terms of the capacity loss the performances of the two cases with the optimized number and ideal infinite number of UCs are actually close. Meanwhile, the case using the optimized number of UCs is obviously much better in cost performance. The developed approach could serve as a general procedure to evaluate the cycle life improvement in other types of batteries when combined with UCs.

## REFERENCES

- [1] J. M. Blanes, R. Gutierrez, A. Garrigós, J. L. Lizán, and J. M. Cuadrado, "Electric vehicle battery life extension using ultracapacitors and an FPGA controlled interleaved buck-boost converter," *IEEE Trans. Power Electron.*, vol. 28, no. 12, pp. 5940–5948, 2013.
- [2] J. C. Schroeder and F. W. Fuchs, "General analysis and design guideline for a battery buffer system with dc/dc converter and EDLC for electric vehicles and its influence on efficiency," *IEEE Trans. Power Electron.*, vol. 30, no. 2, pp. 922–932, 2015.
- [3] J. Shen, S. Dusmez, and A. Khaligh, "Optimization of sizing and battery cycle life in battery/UC hybrid energy storage system for electric vehicle applications," *IEEE Trans. Ind. Inf.*, vol. 10, no. 4, pp. 2112–2121, 2014.

- [4] Z. Song, J. Li, X. Han, L. Xu, L. Lu, M. Ouyang, and H. Hofmann, "Multi-objective optimization of a semi-active battery/supercapacitor energy storage system for electric vehicles," *Appl. Energy*, vol. 135, pp. 212–224, 2014.
- [5] E. Sarasketa-Zabala, I. Gandiaga, E. Martinez-Laserna, L. Rodriguez-Martinez, and I. Villarreal, "Cycle ageing analysis of a LiFePO<sub>4</sub>/graphite cell with dynamic model validations: Towards realistic lifetime predictions," *J. Power Sources*, vol. 275, pp. 573–587, 2015.
- [6] C. G. Hochgraf, J. K. Basco, T. P. Bohn, and I. Bloom, "Effect of ultracapacitor-modified PHEV protocol on performance degradation in lithium-ion cells," *J. Power Sources*, vol. 246, pp. 965–969, 2014.
- [7] B. Scrosati and J. Garche, "Lithium batteries: Status, prospects and future," *J. Power Sources*, vol. 195, no. 9, pp. 2419–2430, 2010.
- [8] L. Lam and P. Bauer, "Practical capacity fading model for li-ion battery cells in electric vehicles," *IEEE Trans. Power Electron.*, vol. 28, no. 12, pp. 5910–5918, 2013.
- [9] N. Omar, M. Daowd, O. Hegazy, P. V. d. Bossche, T. Coosemans, and J. V. Mierlo, "Electrical double-layer capacitors in hybrid topologies-assessment and evaluation of their performance," *Energies*, vol. 5, no. 11, pp. 4533–4568, 2012.
- [10] I. Aharon and A. Kuperman, "Topological overview of powertrains for battery-powered vehicles with range extenders," *IEEE Trans. Power Electron.*, vol. 26, no. 3, pp. 868–876, 2011.
- [11] L. Wang, E. G. Collins, and H. Li, "Optimal design and real-time control for energy management in electric vehicles," *IEEE Trans. Veh. Technol.*, vol. 60, pp. 1419–1429, May 2011.
- [12] T. A. Burress, S. L. Campbell, C. Coomer, C. W. Ayers, A. A. Wereszczak, J. P. Cunningham, L. D. Marlino, L. E. Seiber, and H.-T. Lin, "Evaluation of the 2010 toyota prius hybrid synergy drive system," Oak Ridge National Laboratory (ORNL); Power Electronics and Electric Machinery Research Facility, Tech. Rep., 2011.
- [13] A. Burke and M. Miller, "The UC Davis emerging lithium battery test project," *Institute of Transportation Studies*, 2009.
- [14] —, "The power capability of ultracapacitors and lithium batteries for electric and hybrid vehicle applications," *J. Power Sources*, vol. 196, no. 1, pp. 514–522, 2011.
- [15] Y. Zhang, C.-Y. Wang, and X. Tang, "Cycling degradation of an automotive LiFePO<sub>4</sub> lithium-ion battery," *J. Power Sources*, vol. 196, no. 3, pp. 1513–1520, 2011.
- [16] Z. Li, J. Zhang, B. Wu, J. Huang, Z. Nie, Y. Sun, F. An, and N. Wu, "Examining temporal and spatial variations of internal temperature in large-format laminated battery with embedded thermocouples," *J. Power Sources*, vol. 241, pp. 536–553, 2013.
- [17] T. M. Bandhauer, S. Garimella, and T. F. Fuller, "Temperature-dependent electrochemical heat generation in a commercial lithium-ion battery," *J. Power Sources*, vol. 247, pp. 618–628, 2014.
- [18] C. Freedom, "Battery test manual for power-assist hybrid electric vehicles," DOE/ID-11069, October, Tech. Rep., 2003.
- [19] M. Safari and C. Delacourt, "Aging of a commercial graphite/LiFePO<sub>4</sub> cell," *Journal of the Electrochemical Society*, vol. 158, no. 10, pp. A1123–A1135, 2011.
- [20] J. P. Christophersen, C. D. Ho, C. G. Motloch, D. Howell, and H. L. Hess, "Effects of reference performance testing during aging using commercial lithium-ion cells," *Journal of The Electrochemical Society*, vol. 153, no. 7, pp. A1406–A1416, 2006.